Feedback Control of Many Magnetized *Tetrahymena pyriformis* Cells by Exploiting Phase Inhomogeneity

Aaron Becker, Yan Ou, Paul Kim, Min Jun Kim, and Agung Julius

***Abstract*— Biological robots can be produced in large numbers, but are often controlled by uniform inputs. This makes position control of multiple robots inherently challenging.**

This paper uses magnetically-steered ciliate eukaryon (*Tetrahymena pyriformis*) as a case study. These cells swim at a constant speed, and can be turned by changing the orientation of an external magnetic field. We show that it is possible to steer multiple *T. pyriformis* to independent goals if their turning—modeled as a first-order system—has unique time constants. We provide system identification tools to parameterize multiple cells in parallel.

We construct feedback control-Lyapunov methods that exploit differing phase-lags under a rotating magnetic field to steer multiple cells to independent target positions. We prove that these techniques scale to any number of cells with unique first-order responses to the global magnetic field. We provide simulations steering hundreds of cells and validate our procedure in hardware experiments with multiple cells.

I. Introduction

There are compelling reasons for creating micro-robotics for applications ranging from targeted drug delivery to minimally invasive surgery. The potential impact is broad: large populations of micro-manipulators would enable surgeons to eliminate cancer at the cellular level, let engineers develop complex MEMS assemblies, and empower biologists to simultaneously sort all the cells on a Petri dish. However, the small size of micro- and nano-robots severely limits computation, sensing, and communication. This makes implementing controllers difficult. Building autonomous robots is currently impractical at the micro-scale, making distributed control is infeasible. Centralized approaches are feasible, but individually controlling huge populations of robots requires an equally large amount of communications bandwidth, ultimately limiting the population size. We require a new technique for centralized control under the constraint that every robot receives exactly the same input commands.

This paper applies *ensemble control* to solve this problem [1]. Ensemble control is a control technique that uses a shared input to drive large populations of robots to arbitrary goal states. Our ultimate goal is multi-robot assembly—the fabrication of large, complex structures by hundreds or thousands of robots—with uniform inputs. To make progress, this paper provides a control technique for large numbers of robots with nonholonomic unicycle kinematics where the control input is the desired orientation.

A. Becker is with the Computer Science Department, Rice University, Houston, TX, 77005, USA. Y. Ou and A. Julius are with the Department of Electrical, Computer, and Systems Engineering, Rensselaer Polytechnic Institute, 110 8th Street, Troy, NY 12180, USA. P. Kim and M. Kim are with the Department of Mechanical Engineering and Mechanics, Drexel University, Philadelphia, PA 19104, USA. aabecker@gmail.com, ouy2@rpi.edu,psk25@drexel.edu, mkim@coe.drexel.edu, agung@rpi.edu

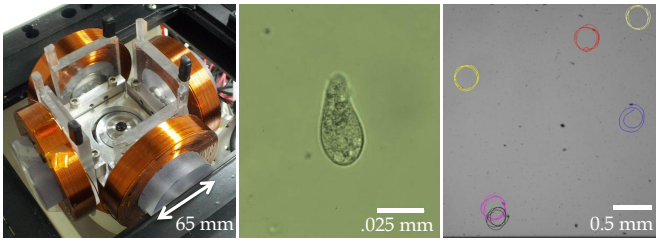

Fig. 1. Using two sets of orthogonal electromagnets (left), Ou et al. demonstrated steering a living magnetized *T. pyriformis* cell [9](middle). In this paper we exploit differences in magnetism between cells to steer multiple cells to arbitrary x, y locations and stabilize them in limit cycles at these locations (six stabilized cells shown at right). See multimedia attachment at http://www.youtube.com/watch?v=MLr2YvghPns.

In previous work [2], [3], we focused on micro/nano-robotic systems with control inputs (forward velocity and turning rate) applied to the *local* coordinate frame, such as electric potential-driven scratch-drive micro-robots [4]–[6] and some light-actuated, molecular nanocar species [7], [8]. These robots have bounded uncertainty in their velocity which scales both their forward velocity and their turning rate. This inhomogeneity allows control of large numbers of robots using the same global signal. We demonstrated that position control is possible for these robots.

Unfortunately, the majority of current micro-robotic systems apply inputs in the *global* coordinate frame. Our system is shown in Figs. 1 and 2. Other examples include magnetic micro/nano robots [10]–[20]; magnetic particles studied by [21]–[24]; magnetic-field controlled bacteria [25]; electric-field controlled paramecium [26], [27]; electrokinetic and optically controlled bacteria [28]; protists steered by magnetic field [9], [29], and electrically driven nano robots [30].

In [4]–[6] the authors designed robots with varying hysteresis levels so that some could orbit in place while others went straight. By cleverly interleaving primitives, they constructed shapes composed of multiple robots. Our biological organisms are more limited: either *all* turn in place, or *all* go straight. Our proof of controllability depends on a control-Lyapunov function. This paper investigates systems where the inputs are the desired heading, encoded by a global vector field. We focus on artificially magnetotactic *Tetrahymena pyriformis* cells and model them as controllable microrobots. *T. pyriformis* are eukaryotic, pear-shaped cells, ≈50 μm long by 25 μm wide. These cells swim using the numerous cilia that cover their cell bodies. *T. pyriformis* can be grown

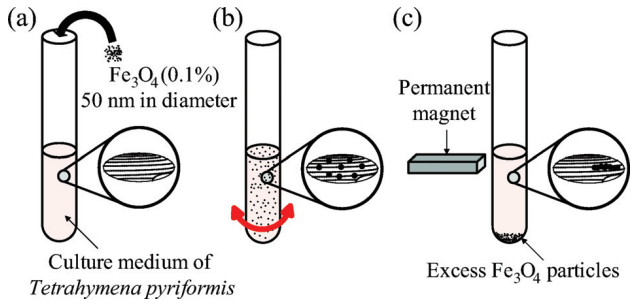

Fig. 2. The procedure for the fabrication of artificially magnetotactic *T. pyriformis*. (a) Addition of iron oxide particles (magnetite, Fe_3O_4) into the culture medium. (b) Gentle agitation to ensure the cells internalize the iron oxide particles. (c) Magnetization of the internalized particles using a permanent magnet. Reproduced from Kim et al. (2011).

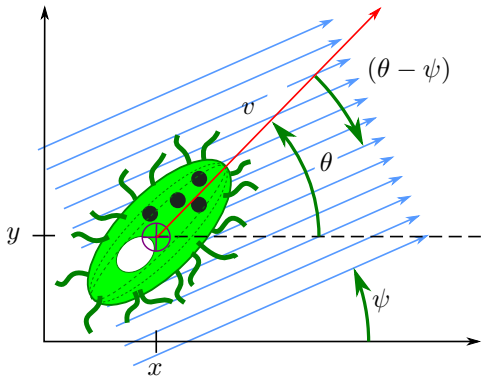

Fig. 3. Kinematic model of a magnetized *T. pyriformis* cell. The magnetic field exerts a torque $Ma(\theta - \psi)$ to align the cell axis θ with the field ψ.

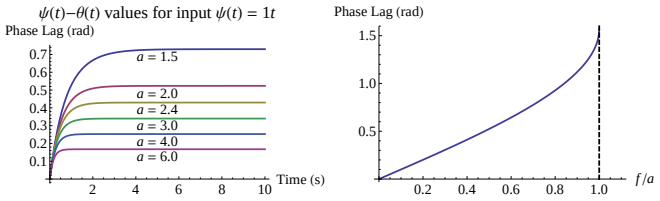

Fig. 4. A cell modeled by (1), under a constantly rotating magnetic field $\psi(t) = ft$ will reach a steady-state phase lag of $\arcsin(\frac{f}{a})$ radians. $f = Ma$ is the *step-out frequency*, after which the phase lag grows without bound. This growth is approximately linear.

in large quantities in the laboratory with ease. They have been studied under the influence of various *taxes*, the innate behavioral response by an organism to a directional stimulus. Galvanotactic control of *T. pyriformis* has been investigated by Kim et al. [32]. Kim et al. also used magnetic fields to control the motion of a *T. pyriformis* by feeding iron-particles into the cell body [32]. Feedback control of single cell has been developed using rapidly-exploring random trees (RRTs) [33] and model predictive control (MPC) [34], [35]. These results show promise, but for large-scale micro-assembly and micro-manipulation, single-cell motion control is not sufficient. We require a control technique that can use a global magnetic field to simultaneously control many cells.

The paper is structured as follows. First, we introduce our model for the system (Section II), next we prove this system is controllable and provide a feedback control law (Section III), validate this control law in simulation and hardware experiments (Section IV), and finish with concluding remarks (Section V).

II. Modeling

For modeling we will work with a simplified 2D approach that ignores the effects of gravity and collisions. Both are well documented, and their effects on control strategies warrants further study. Gravity alone would not make the system ensemble controllable, but boundary effects may. Disturbances from robot-robot interactions are also ignored, and may be significant. Extending the model to 3D requires additional states and motion primitives, similar to those used for 2D.

Let the model for the ith cell shown in Figure 3, with turning time constant a_i, be

$$\begin{bmatrix} \dot{x}_i \\ \dot{y}_i \\ \dot{\theta}_i \end{bmatrix} = \begin{bmatrix} v_i \cos\theta_i \\ v_i \sin\theta_i \\ Ma_i \sin(\psi - \theta_i) \end{bmatrix} \tag{1}$$

Here the x_i, y_i are Cartesian coordinates, θ_i is the orientation of the cell, ψ is the orientation of the magnetic field, and v_i is the swimming speed of the cell. The cell is pulled to orient along the magnetic field ψ by a magnetic field of magnitude M, and the rate of this alignment is given by the parameter a_i. We assume the relationship is first order for some range about 0 and thus can be modeled as an ideal torsional spring. As long as the magnetic field is on, in steady-state a large group of magnetized cells will share the same orientation. No steady-state dispersion in orientation is possible when a magnetic field is present. It may be possible to command a change in ψ, quickly turn off the magnetic field, and get a distribution of orientations parameterized by a, but this dispersion will vanish when the magnetic field is replaced.

The nonlinear term $\sin(\theta - \psi)$ is due to the periodicity of the magnetic torque. For small $|\theta - \psi|$ we can use the small-angle approximation $(\theta - \psi)$.

A. Constantly Rotating Magnetic Field

As shown previously, to make multiple cells controllable by the same magnetic field, we must exploit heterogeneity in turning rate. One method is by using a constantly rotating magnetic field $\psi(t) = ft$, where $f \in \mathbb{R}^+$ is the frequency of rotation. For $f < Ma$, the cells will reach a steady-state phase lag as they attempt to align with the field. At steady-state the cells are turning at the same speed as the magnetic field

$$\begin{aligned} \dot{\theta}_i &= Ma_i \sin\left(\theta_i(t) - \psi(t)\right) \\ f &= Ma_i \sin\left(\theta_i(t) - ft\right) \\ \arcsin(\frac{f}{Ma_i}) &= \theta_i(t) - ft. \end{aligned} \tag{2}$$

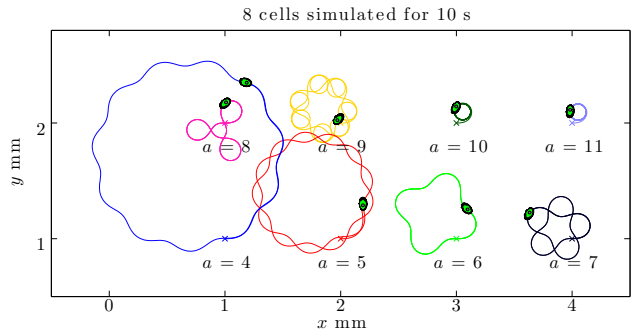

Fig. 5. Limit-cycles for cells with different a values at $f = 10$ rad/s.

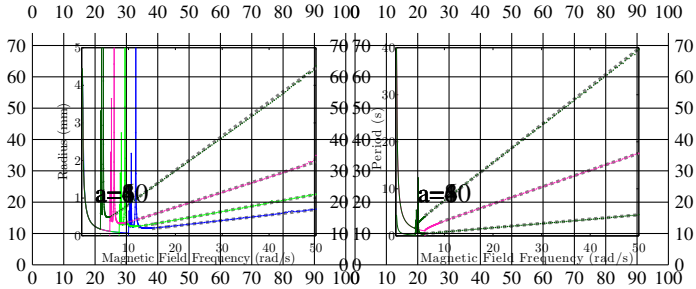

Fig. 6. As the magnetic field frequency f increases, the radius the cell swims in and the period of rotation decrease in a reciprocal relationship until a, the cutoff frequency. The radius values are erratic from a to $1.5a$, but after $1.5a$ are linear in a^2 (a linear-fit line is in dashed grey: $r = 1.45f/a^2 + -0.3/a$, $T = 12.9f/a^2 - 2.3/a$). Shown are $a = [4, 6, 8, 10]$.

This steady-state phase lag is shown in Fig. 4. The quantity $\frac{f}{Ma_i}$ is the *step-out frequency*, after which the phase lag grows without bound. This growth is approximately linear for $f > 1.5a$, as shown in Fig. 6. The effective period for the cell is

$$T_i = \begin{cases} \frac{2\pi}{f} & \text{if } f < Ma_i \\ \approx 12.9f(Ma_i)^{-2} - 2.3(Ma_i)^{-1} & \text{else} \end{cases} \tag{3}$$

We can also compute the effective radius of the limit cycle the cell follows. For $f < a$, the cell completes a cycle every $2\pi/f$ seconds and the radius is therefore v/f. Past the step-out frequency, the cells turn in periodic orbits similar to the hypotrochoids and epitrochoids produced by a Spirograph toy. Representative limit cycles are shown in Fig. 5. The radius of rotation is:

$$r_i = \begin{cases} \frac{v_i}{f} & \text{if } f < Ma_i \\ \approx 1.45f(Ma_i)^{-2} - 0.3(Ma_i)^{-1} & \text{else} \end{cases}$$

B. Arbitrary Orientations

If we could control the orientation of each cell independently, the cells could swim directly to the goal. Fig. 7 shows two cells with different a parameters. If the rotation frequency f and the a values are coprime, the range of possible θ_1 and θ_2 values span $[0, 2\pi] \times [0, 2\pi]$. By increasing f we can control the density we sample these angles. The right side of Fig. 7 shows that the time required to span $[0, 2\pi] \times [0, 2\pi]$ increases with f.

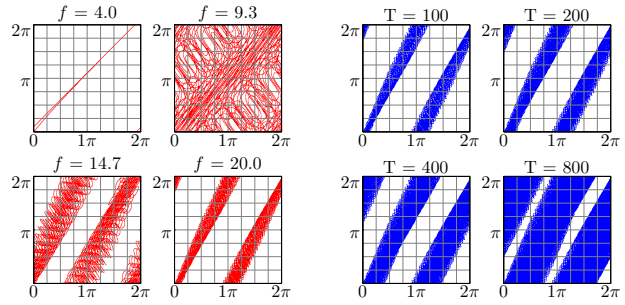

Fig. 7. Shown are the heading angles for two cells with $a = \{5, 7\}$. The x axis is θ_1, y axis θ_2. Left: simulation for 100 s at increasing rotation frequencies f of the external magnetic field. If f and the a values are coprimes, the possible angular values span $[0, 2\pi] \times [0, 2\pi]$. Right: rotation frequency of the external magnetic field $f = 20$ simulated for increasing amounts of time. As time increases, the set of possible angular value pairs becomes dense.

C. Straight-Line Swimming

By turning the magnetic field off, the cell dynamic model simplifies to

$$\begin{bmatrix} \dot{x}_i \\ \dot{y}_i \\ \dot{\theta}_i \end{bmatrix} = \begin{bmatrix} v_i \cos\theta_i \\ v_i \sin\theta_i \\ 0 \end{bmatrix} \tag{4}$$

Without an external magnetic field, the cells swim straight in the direction they were headed when the magnetic field was last on. If we store the orientation of the magnetic field when the magnetic field is turned off at time t_a as $\psi_a = ft_a$, then when we turn the field back on at time t_b we can resume where we last stopped

$$\psi(t) = \psi_a + f(t - t_b),$$

and the cells will continue their limit-cycle behavior, but the center of rotation will be translated $v_i(t_b - t_b)$ along the vector $\theta_i(t_a)$.

D. System Identification

Our previous technique for system identification required manual control of the magnetic field by a human user to keep a single cell within the field of view (FOV). Human control does not scale to many cells because their differing speeds makes it very challenging to maintain even two cells within the FOV long enough to perform system identification. Our new approach involves using a constantly-rotating magnet field to hold the cells in periodic limit cycles. We can then analyze the vision data and directly measure the v_i and a_i values from the phase lag and the radius of rotation using (2) and (5).

III. Feedback Control

Our control input consists of an alternating sequence of ORBIT and SWIM-STRAIGHT modes. The oscillation frequency f of the magnetic field is constant for every ORBIT mode. At the beginning of each ORBIT mode, the phase of the magnetic oscillation is resumed from the previous ORBIT mode. During the first ORBIT mode, we identify the

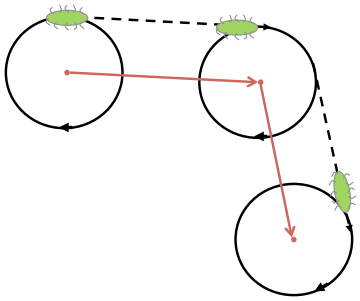

Fig. 8. Our control input consists of an alternating sequence of ORBIT and SWIM-STRAIGHT modes. our algorithms choose the switching time to move the center of rotation $(x_{c,i}, y_{c,i})$ toward a goal position.

centers of rotation $(x_{c,i}, y_{c,i})$ of each cell by recording the cell positions for at least one period, calculated by (3), and computing

$$x_{c,i}(t) = \max\big(x_i(t-T:t)\big) - \min\big(x_i(t-T:t)\big)$$
$$y_{c,i}(t) = \max\big(y_i(t-T:t)\big) - \min\big(y_i(t-T:t)\big). \quad (5)$$

The center of rotation of each cell translates along with the cell during each SWIM-STRAIGHT mode (see Fig. 8).

A. Control-Lyapunov Function

We will use these two behaviors, constant rotation and straight-line swimming, to design a control-Lyapunov function

Theorem 3.1: The ensemble (1) with unique a_i values is is globally asymptotically stabilizable.

We will prove global asymptotic stability by using a control-Lyapunov function [36]. This proof provides a control law that decreases the position error whenever it is possible to do so by toggling the magnetic field M. Without loss of generality, we will assume the goal position is the origin. A suitable Lyapunov function is the squared distance of the center of rotation, $[x_{c,i}, y_{c,i}]$ (5), from the origin:

$$V(t,x,y) = \frac{1}{2}\sum_{i=1}^{n}\left(x_{c,i}^2(t) + y_{c,i}^2(t)\right) \quad (6)$$

The derivative of $V(t,x,y)$ is

$$\dot{V}(t,x,y) = \begin{cases} \sum_{i=1}^{n} \left(x_{c,i}(t)\dot{x}_i(t) \right. \\ \qquad \left. + y_{c,i}(t)\dot{y}_i(t)\right) & \text{if } M = 0 \\ 0 & \text{else} \end{cases}$$
$$= \begin{cases} \sum_{i=1}^{n} v_i \left(x_{c,i}(t)\cos\theta_i(t) \right. \\ \qquad \left. + y_{c,i}(t)\sin\theta_i(t)\right) & \text{if } M = 0 \\ 0 & \text{else} \end{cases}$$
$$= \begin{cases} F(t) & \text{if } M = 0 \\ 0 & \text{else} \end{cases} \quad (7)$$

We note here that $V(t,x,y)$ is both positive definite and is radially unbounded, and $V(t,x,y) \equiv 0$ only at $[x_{c,i}, y_{c,i}] = [0,0]$.

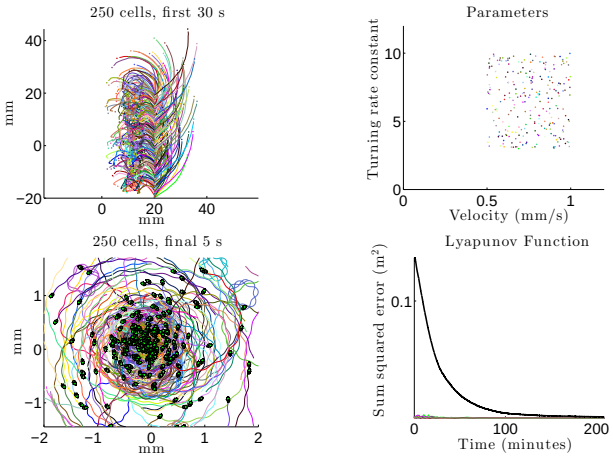

Fig. 9. 250 cells initialized at $x = 20$ mm, y evenly spaced $[-20, 20]$ mm, with v_i, a_i values distributed uniformly randomly in $[0.5, 1]mm/s \times [3, 10]$ under control law (8) with threshold (9).

B. Choosing a Control Law

Our controller consists of deciding when to turn the magnetic field M on. To make $\dot{V}(t,x,y)$ negative semi-definite, we choose

$$M(t) = \begin{cases} 0 & \text{if } F(t) < \text{threshold} \\ 1 & \text{else} \end{cases} \quad (8)$$

for some $\text{threshold} \leq 0$ value. With such a $M(t)$, whenever $M(t) = 0$, the Lyapunov function is decreasing at a rate $\leq \text{threshold} \leq 0$. Note here that $\dot{V}(t,x,y) \leq 0$, but there exists a subspace of $[x_i(t), y_i(t)]$ such that $\dot{V}(t,x,y) = 0$. Because $\dot{V}(t,x,y)$ is negative semi-definite, we can only claim stability, not asymptotic stability. To gain a proof of asymptotic stability, we must choose a threshold function such that M is always nonzero only at the origin.

We present three candidate threshold functions.

a) GREEDY: The GREEDY approach switches to straight-line driving whenever the straight-line driving will reduce the error faster than a threshold based on the current distance from the goal

$$\text{threshold} = -\frac{1}{2}\sum_{i=1}^{n} v_i \sqrt{x_{c,i}(t)^2 + y_{c,i}(t)^2}. \quad (9)$$

This approach scales to any number of cells and is robust to noise. Simulated results with 250 cells are shown in Fig. 9. The time required for convergence as a function of the number of cells is shown in Fig. 10, and appears to grow linearly. Unfortunately, this approach requires rapidly turning the magnetic field on and off. A magnetic field with a large time constant cannot faithfully implement this controller. A second potential problem is that while this controller monotonically reduces the sum of squared errors, it may not monotonically reduce the squared error for each individual cell—a small fraction of the cells may temporarily move away from their goals. The next controllers alleviate these problems.

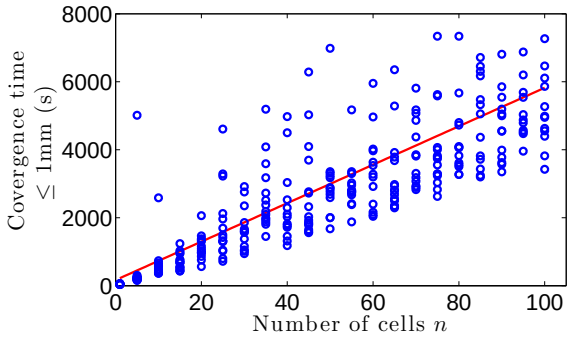

Fig. 10. Convergence time as a function of population size for simulated cells. Cells initializes at $x = 20$ mm, y evenly spaced $[-20, 20]$ mm, with v_i, a_i values distributed uniformly randomly in $[0.5, 1]mm/s \times [3, 10]$ under control law (8) with threshold (9). The best-fit line slope is 57s/robot.

b) STEEPESTDESCENT: The STEEPESTDESCENT approach only switches to straight-line driving when all the cell's headings point toward the target. This maximizes the gradient of the Lyapunov function. It is generally difficult, and often impossible to make all the cells head directly to the target, so we set a tolerance region for the mean squared angular error

$$\frac{1}{n}\sum_{i=1}^{n} \arctan2\big(\sin(\theta_i(t) - \theta_{i,target}), \cos(\theta_i(t) - \theta_{i,target})\big)^2 < tolerance_{SD}$$

Because the cells all have different speeds v_i, they do not arrive at the target at the same time. As cells overshoot the target, the Lyapunov function increases. We use the threshold value in (9) to resume constant rotation.

This approach is designed to minimize the required field of view because the experimental setup FOV is limited. Fig. 11 compares the GREEDY and STEEPESTDESCENT controllers. The STEEPESTDESCENT approach is unsuited for controlling large populations (more than 5 cells). Aligning n cells at desired heading angles is demonstrated in Fig. 6, and quickly becomes challenging as n increases. STEEPESTDESCENT provides favorable results in simulations with two cells.

c) HYBRID: The HYBRID approach attempts to combine the advantages of feedback ensemble control and a constant magnetic field. With a constant magnetic field, all the cells swim along the same heading angle. We can use a constant magnetic field to control the mean position of a large group of cells. In our future applications we want to use large numbers of cells to manipulate objects. The force applied to an object is proportional to the number of cells that can be brought in contact with the object with the same heading angle, and a constant magnetic field allows all the

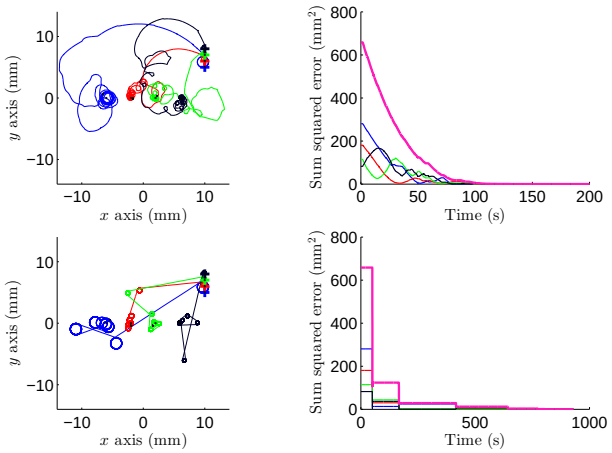

Fig. 11. Left: simulation trajectory of four cells under GREEDY and STEEPESTDESCENT feedback control. The cells start in a vertical line at $\{[10, 5], [10, 6], [10, 7], [10, 8]\}$ mm and are steered to orbit goal positions in a horizontal line at $\{[-6, 0], [-2, 0], [2, 0], [6, 0]\}$ mm. The magnetic field has frequency 15 rad/s, the a values are $\{5, 6, 7, 8\}$, and the speeds v are $\{0.8, 0.5, 0.6, 0.7\}$ mm/s. These tests required $\{200, 930\}$ s for all cells to converge within 0.2 mm of their goal positions. Right: Lyapunov function (sum squared distance error) of the four cells as a function of time.

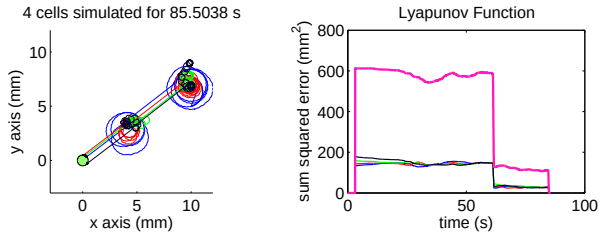

Fig. 12. Preliminary study on manipulation using multiple cells to push a micro-structure. Left: simulation trajectory of four cells under the HYBRID feedback control algorithm. The cells have the same initial positions and parameters as in Fig. 11, but the control objective is to push a 0.5 mm radius disc centered at $[0, 0]$ and drawn in green. This simulation required 85.5 s to reach the disc. Right: Lyapunov function (sum squared distance error) of the four cells as a function of time.

cells to push in the same vector direction.

$$\bar{x} = \frac{1}{n}\sum_{i=1} x_i, \qquad \bar{y} = \frac{1}{n}\sum_{i=1} y_i,$$
$$s_x = \frac{1}{n}\sum_{i=1} (x_i - \bar{x})^2, \qquad s_y = \frac{1}{n}\sum_{i=1} (y_i - \bar{y})^2,$$
$$\sigma = \sqrt{s_x + s_y} > tolerance_H$$

The HYBRID approach uses a rotating magnetic field to gather cells together and uses an unchanging magnetic field to swim cells to the target. In this case, if the cells' positions are too sparse and exceed $tolerance_H$, we gather the cells using GREEDY or STEEPESTDESCENT by defining the target as $(\bar{x}, \bar{y})$. Once the cells gather within $tolerance_H$, we switch to a constant magnetic field and the cells swim in unison toward the target. This technique could be used as a primitive operation for micro-manipulation tasks. Figure 12 shows a simulation where multiple cells are steered to push a disc.

Comparison	GREEDY	STEEPEST-DESCENT	HYBRID
Convergence	fastest	slower	slowest
Max. robots	∞	$n \leq 5$	$n \leq 5$
Robustness	constant corrections	N/A	straight-line movement with magnetic field
Field of view	may increase	never increases	never increases
Uniform movement	no	no	yes
Toggling mag. field	often	rarely	rarely

TABLE I

COMPARISON OF THE THREE CONTROL STRATEGIES.

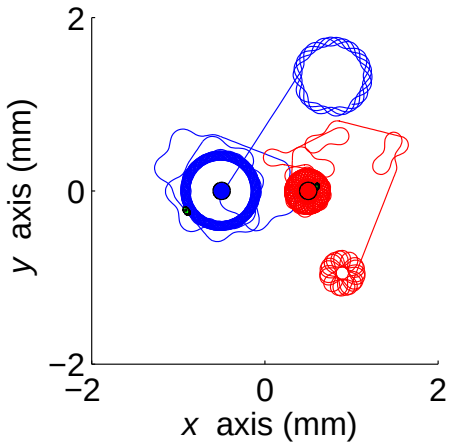

Fig. 13. Feedback control of two simulated cells within a limited (2×2 mm) field of view. The cells start at [1,1],[1,-1]mm and are steered to orbit goal positions [-0.5,0],[0.5,0]. The magnetic field frequency is 11 rad/s, $a = \{6, 8\}$, and speed $v = \{0.8, 0.75\}$ mm/s. The cells required 122 s to converge within 0.2 mm of their goal positions

IV. VALIDATION

Simulation results for Eq. (1) are promising. For hardware experiments, the mathematical models must first be calibrated to match magnetized cells.

In this section we compare three control schemes, GREEDY, STEEPESTDESCENT, and HYBRID.

Each simulation uses cells with identical turning rates a, velocities v, and initial positions and orientations. In each test, the cells were successfully steered to end within 2 mm of the origin. These results are representative: the time consumption for algorithm one is the smallest, since this method does not require the cells to spin until all the cells are oriented toward the goal. The second and third feedback ensemble control methods require a smaller field of view to gather cells to the target. This is important because the field of view is limited in our experimental setup. The third feedback ensemble control algorithm has advantage in applying a magnetic field to make the cells head to the target. In this case, the cells will move in the same vector direction, which may be useful for micromanipulation tasks. It has the slowest convergence time, but it uses a constant magnetic field for straight-line movement, which will ensure the cells move in a straight line.

Our experimental setup has a field of view 5×3.25 mm. The test shown in Fig. 13 suggests that our algorithm could control two cells within this limited field of view.

A. Hardware Setup

T. pyriformis are cultured in solution of 1% (w/v) tryptone (Sigma Aldrich) and 0.1% (w/v) yeast extract (Sigma Aldrich) and incubated at $28\,^{\circ}\mathrm{C}$. Cells are innoculated weekly.

Cells were placed in a multi-functional orthogonal coil chamber, where two pairs of electromagnets are evenly spaced, as shown in Fig. 1, with each pair corresponding to the x and y axes. Variable rotating magnetic fields are supplied using inputs from two power supplies controlled with LabView software and National Instruments controllers. The chamber is placed on a stage of an inverted microscope (Leica DM IRB), where samples are observed through a $4\times$ objective. Images are captured using a Photron Fastcam SA-3 high-speed camera at 125 frames per second. Cells are placed inside a PDMS microfluidic channel measuring 3 mm wide and 100 μm deep.

In these experiments, we must avoid large magnetic fields M. Under large M, turning rapidly in circles damages cells when the internalized iron-oxide particles rotate quickly inside the body, resulting in abnormal swimming.

B. Hardware Experiments: System Identification

To choose the optimal frequency of the rotation magnetic field requires knowing the a values for the set of cells we want to control. We employ the method of least squares to determine the a values. First we discretize the continuous plant model (1)

$$\begin{bmatrix} x_i(k+1) \\ y_i(k+1) \\ \theta_i(k+1) \end{bmatrix} = \begin{bmatrix} v_i \Delta T \cos\theta_i(k) \\ v_i \Delta T \sin\theta_i(k) \\ M\alpha \sin(\psi(k) - \theta_i(k)) \end{bmatrix}, \quad (10)$$

where ΔT is the sampling time and $\alpha \approx \Delta T$.

To identify the α parameter for each cell, we record position and orientation measurements under a constantly rotating magnetic field. We record the discrete-time cell orientation information as $\theta_i(0), \theta_i(1), \ldots, \theta_i(k), \ldots, \theta_i(n)$, and the magnetic field orientation as $\psi(0), \psi(1), \ldots, \psi(k), \ldots, \psi(n)$. The following equation is derived from (10).

$$\begin{bmatrix} \theta_i(1) - \theta_i(0) \\ \theta_i(2) - \theta_i(1) \\ \vdots \\ \theta_i(k) - \theta_i(k-1) \\ \vdots \\ \theta_i(n) - \theta_i(n-1) \end{bmatrix} = \begin{bmatrix} \sin(\psi(0) - \theta_i(0)) \\ \sin(\psi(1) - \theta_i(1)) \\ \vdots \\ \sin(\psi(k-1) - \theta_i(k-1)) \\ \vdots \\ \sin(\psi(n-1) - \theta_i(n-1)) \end{bmatrix} \cdot \alpha. \quad (11)$$

We rewrite this equation as $Y = \Phi\alpha$. Then, using the method of least squares, the parameter set with the best fit to the data is given by $\hat{\alpha} = \Phi^{\dagger} Y$, where $\Phi^{\dagger} = (\Phi^T \Phi)^{-1} \Phi^T$ is

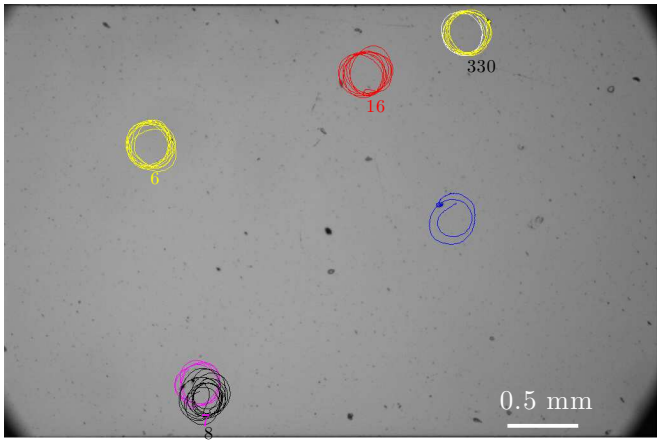

Fig. 14. Under a constantly rotating magnetic field, *T. pyriformis* cells follow circular limit-cycles. We record position as a function of time and the magnetic-field phase, and process this data to perform system identification of multiple cells in parallel. In the frame above, we identified the a and v parameters for five cells.

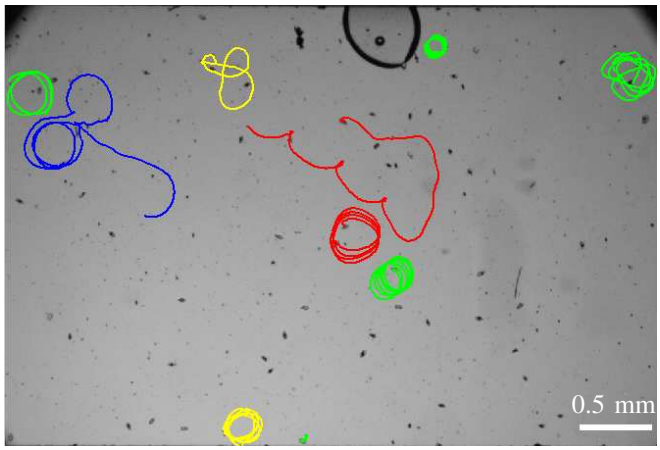

Fig. 15. Experimental results for nine *T. pyriformis* cells under the influence of a magnetic field rotating at 6 rad/s. The cells turn in tight limit cycles, as predicted by our model. The field was on for a duration of 6.6 seconds.

the pseudoinverse of Φ. The a value of cell is derived as $a = \frac{\alpha}{\Delta T}$.

The a value can also be measured directly by inverting (2). If the frequency of the rotation magnetic field is below the step-out frequency, the cells turn in a circle with a constant phase lag $\theta_{i,lag}$. The turning-rate parameter is then $a_i = -f/\sin(\theta_{i,lag})$.

From the experimental data shown in Fig. 14, we identify for cells numbered $\{6, 7, 8, 16, 330, \}$, a values $\{5.82, 2.94, -8.56, 5.45, -5.45\}$ and speeds $\{172, 155, 133, 165, 167\}$ px/s. In our setup each pixel is 0.23 μm wide, giving speeds $\{39.6, 35.7, 30.638.0, 38.4\}$ μm/s.

T. pyriformis cells do follow periodic orbits under a constantly rotating magnetic field. Fig. 15 shows cells under the influence of a magnetic field rotating at 6 rad/s. The cells turn in tight limit cycles, as predicted by our model (1).

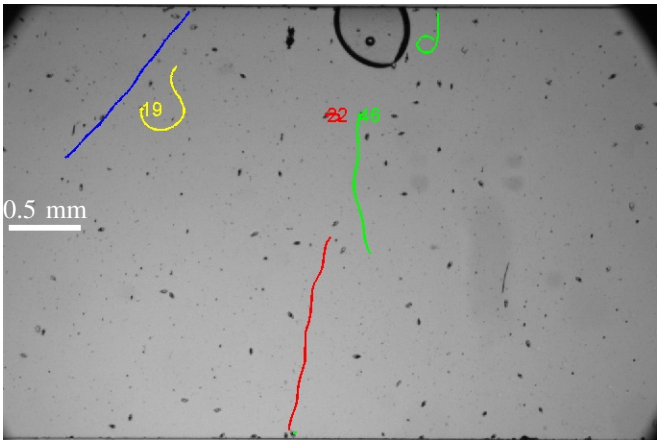

Fig. 16. This frame shows the paths traveled by six cells from Fig. 15 after turning the magnetic field off. A majority of the cells swim in a straight line. The path traces show 1.6 seconds of movement.

C. Hardware Experiments: Straight-Line Swimming

Fig. 16 shows the paths traveled by six cells from the previous experiment, after turning the magnetic field off. A majority (62%) of the cells swim in a straight line. The path traces show 1.6 seconds of movement.

V. Conclusion

We have provided an algorithm for steering multiple micro-robots to arbitrary ending positions when the only control input is the global desired heading. We demonstrated a technique for performing model-learning on a large epopulation of cells simultaneously, using video data.

An obvious extension is to apply this work to artificial micro robots controlled by magnetic fields [10]–[19], [21]–[24]. In many of these systems [16] the robot speed is also controllable, allowing the robots to be turned in-place.

These results can be directly extended to 3D by augmenting the state and error signals with z and using angles in $SO(3)$. This can be implemented trivially by first using control laws from Section III to move to desired x, y positions, and finish by moving to the desired z positions, requiring $\approx 1.5\times$ as many operations as in 2D.

Preliminary hardware experiments with multiple cells are promising. This paper represents a step toward our future goal of using multiple cells to manipulate many objects simultaneously.

VI. Acknowledgements

This work was supported by the National Science Foundation under CMMI 1000255, CMMI 1000284, and by ARO W911F-11-1-0490.

References

[1] J.-S. Li and N. Khaneja, "Ensemble control of Bloch equations," *IEEE Trans. Autom. Control*, vol. 54, no. 3, pp. 528–536, Mar. 2009.

[2] A. Becker, "Ensemble control of robotic systems," Ph.D. dissertation, University of Illinois at Urbana-Champaign, http://hdl.handle.net/2142/34221, Aug. 2012.

[3] A. Becker, C. Onyuksel, and T. Bretl, "Feedback control of many differential-drive robots with uniform control inputs," in *IEEE/RSJ International Conference on Intelligent Robots and Systems (IROS)*, Oct. 2012.

[4] B. Donald, C. Levey, and I. Paprotny, "Planar microassembly by parallel actuation of MEMS microrobots," *J. of MEMS*, vol. 17, no. 4, pp. 789–808, Aug. 2008.

[5] I. Paprotny, C. Levey, and B. Donald, "Turning-rate selective control: A new method for independent control of stress-engineered MEMS microrobots," in *Robotics: Science and Systems (RSS)*, vol. VIII, Sydney, Australia, Jul. 2012.

[6] B. R. Donald, C. G. Levey, I. Paprotny, and D. Rus, "Planning and control for microassembly of structures composed of stress-engineered mems microrobots," *The International Journal of Robotics Research*, vol. 32, no. 2, pp. 218–246, 2013. [Online]. Available: http://ijr.sagepub.com/content/32/2/218.abstract

[7] Y. Shirai, A. J. Osgood, Y. Zhao, K. F. Kelly, and J. M. Tour, "Directional control in thermally driven single-molecule nanocars," *Nano Letters*, vol. 5, no. 11, pp. 2330–2334, Feb. 2005.

[8] P.-T. Chiang, J. Mielke, J. Godoy, J. M. Guerrero, L. B. Alemany, C. J. Villagómez, A. Saywell, L. Grill, and J. M. Tour, "Toward a light-driven motorized nanocar: Synthesis and initial imaging of single molecules," *ACS Nano*, vol. 6, no. 1, pp. 592–597, Feb. 2011.

[9] Y. Ou, D. H. Kim, P. Kim, M. J. Kim, and A. A. Julius, "Motion control of magnetized tetrahymena pyriformis cells by magnetic field with model predictive control," *Int. J. Rob. Res.*, vol. 32, no. 1, pp. 129–139, Jan. 2013.

[10] J. J. Abbott, K. E. Peyer, M. C. Lagomarsino, L. Zhang, L. X. Dong, I. K. Kaliakatsos, and B. J. Nelson, "How should microrobots swim?" *Int. J. Rob. Res.*, July 2009, doi:10.1177/0278364909341658.

[11] D. Frutiger, B. Kratochvil, K. Vollmers, and B. J. Nelson, "Magmites - wireless resonant magnetic microrobots," in *IEEE Int. Conf. Rob. Aut.*, Pasadena, CA, May 2008.

[12] H.-W. Tung, D. R. Frutiger, S. Panè, and B. J. Nelson, "Polymer-based wireless resonant magnetic microrobots," in *IEEE International Conference on Robotics and Automation*, May 2012, pp. 715–720.

[13] M. P. Kummer, J. J. Abbott, B. Kratochvil, R. Borer, A. Sengul, and B. J. Nelson, "Octomag: An electromagnetic system for 5-dof wireless micromanipulation," *IEEE Trans. Robot.*, vol. 26, no. 6, pp. 1006–1017, 2010.

[14] S. Schürle, K. E. Peyer, B. E. Kratochvil, and B. J. Nelson, "Holonomic 5-DOF magnetic control of 1D nanostructures," in *IEEE Int. Conf. Rob. Aut.*, May 2012, pp. 1081–1086.

[15] S. Tottori, L. Zhang, F. Qiu, K. Krawczyk, A. Franco-Obregón, and B. J. Nelson, "Magnetic helical micromachines: Fabrication, controlled swimming, and cargo transport," *Advanced Materials*, vol. 24, no. 811, 2012.

[16] L. Zhang, J. J. Abbott, L. X. Dong, B. E. Kratochvil, H. X. Zhang, K. E. Peyer, and B. J. Nelson, "Micromanipulation using artificial bacterial flagella," in *Proc. of IEEE/RSJ International Conference on Intelligent Robots and Systems (IROS)*, St. Louis, MO, USA, Oct. 2009.

[17] E. Diller, S. Floyd, C. Pawashe, and M. Sitti, "Control of multiple heterogeneous magnetic microrobots in two dimensions on nonspecialized surfaces," *IEEE Trans. Robot.*, vol. 28, no. 1, pp. 172–182, Feb. 2012.

[18] S. Floyd, E. Diller, C. Pawashe, and M. Sitti, "Control methodologies for a heterogeneous group of untethered magnetic micro-robots," *Int. J. Robot. Res.*, vol. 30, no. 13, pp. 1553–1565, Nov. 2011.

[19] P. Vartholomeos, M. Akhavan-Sharif, and P. E. Dupont, "Motion planning for multiple millimeter-scale magnetic capsules in a fluid environment," in *IEEE Int. Conf. Rob. Aut.*, May 2012, pp. 1927–1932.

[20] E. B. Steager, M. Selman Sakar, C. Magee, M. Kennedy, A. Cowley, and V. Kumar, "Automated biomanipulation of single cells using magnetic microrobots," *The International Journal of Robotics Research*, vol. 32, no. 3, pp. 346–359, 2013. [Online]. Available: http://ijr.sagepub.com/content/32/3/346.abstract

[21] M. Belkin, A. Snezhko, I. S. Aranson, and W.-K. Kwok, "Driven magnetic particles on a fluid surface: pattern assisted surface flows." *Phys Rev Lett*, vol. 99, no. 15, p. 158301, 2007. [Online]. Available: http://www.biomedsearch.com/nih/Driven-magnetic-particles-fluid-surface/17995219.html

[22] A. Snezhko, I. S. Aranson, and W.-K. Kwok, "Surface wave assisted self-assembly of multidomain magnetic structures." *Phys Rev Lett*, vol. 96, no. 7, p. 078701, 2006. [Online]. Available: http://www.biomedsearch.com/nih/Surface-wave-assisted-self-assembly/16606148.html

[23] A. Snezhko, M. Belkin, I. S. Aranson, and W.-K. Kwok, "Self-assembled magnetic surface swimmers." *Phys Rev Lett*, vol. 102, no. 11, p. 118103, 2009. [Online]. Available: http://www.biomedsearch.com/nih/Self-assembled-magnetic-surface-swimmers/19392241.html

[24] C. Orduño, A. Becker, and T. Bretl, "Motion primitives for path following with a self-assembled robotic swimmer," in *IEEE Int. Rob. and Sys.*, Oct. 2012.

[25] O. Felfoul, M. Mohammadi, L. Gaboury, and S. Martel, "Tumor targeting by computer controlled guidance of magnetotactic bacteria acting like autonomous microrobots," in *Intelligent Robots and Systems (IROS), 2011 IEEE/RSJ International Conference on*, 2011, pp. 1304–1308.

[26] K. Hashimoto, K. Takahashi, N. Ogawa, and H. Oku, "Visual feedback control for a cluster of microorganisms," in *International Joint Conference SICE-ICASE*, Oct. 2006, pp. 4198–4201.

[27] T. Hasegawa, N. Ogawa, H. Oku, and M. Ishikawa, "A new framework for microrobotic control of motile cells based on high-speed tracking and focusing," in *IEEE Int. Conf. Rob. Aut.*, May 2008, pp. 3964–3969.

[28] E. B. Steager, M. Sakar, D. H. Kim, V. Kumar, and G. J. Pappas, "Electrokinetic and optical control of bacterial microrobots." *J. of Micromechanics and Microengineering*, vol. 21, no. 3, Mar. 2011.

[29] Y. Ou, D. H. Kim, P. Kim, M. J. Kim, and A. A. Julius, "Motion control of tetrahymena pyriformis cells with artificial magnetotaxis: Model predictive control (MPC) approach," in *IEEE Int. Conf. Rob. Aut.*, May 2012, pp. 2492–2497.

[30] T. Kudernac, N. Ruangsupapichat, M. Parschau, B. Maci'a, N. Katsonis, S. R. Harutyunyan, K.-H. Ernst, and B. L. Feringa, "Electrically driven directional motion of a four-wheeled molecule on a metal surface," *Nature*, vol. 479, no. 7372, pp. 208–211, Nov. 2011.

[31] Q. Wang, Y. Ou, A. A. Julius, K. L. Boyer, and M. J. Kim, "Tracking tetrahymena pyriformis cells using decision trees," in *Pattern Recognition (ICPR), 2012 21st International Conference on*, Nov., pp. 1843–1847.

[32] D. H. Kim, U. K. Cheang, L. K̈hidai, D. Byun, and M. J. Kim, "Artificial magnetotactic motion control of tetrahymena pyriformis using ferromagnetic nanoparticles: A tool for fabrication of microbiorobots," *Applied Physics Letters*, vol. 97, no. 17, p. 173702, 2010. [Online]. Available: http://link.aip.org/link/?APL/97/173702/1

[33] D. H. Kim, S. Brigandi, A. A. Julius, and M. J. Kim, "Real-time feedback control using artificial magnetotaxis with rapidly-exploring random tree (RRT) for *Tetrahymena pyriformis* as a microbiorobot," in *Robotics and Automation (ICRA), 2011 IEEE International Conference on*, may 2011, pp. 3183 –3188.

[34] Y. Ou, D. H. Kim, P. Kim, M. J. Kim, and A. A. Julius, "Motion Control of *Tetrahymena pyriformis* Cells with Artificial Magnetotaxis: Model Predictive Control (MPC) Approach," *to appear in Robotics and Automation (ICRA), 2012 IEEE International Conference, St. Paul, USA*, 2012.

[35] ——, "Motion control of magnetized Tetrahymena pyriformis cells by magnetic field with Model Predictive Control," *International Journal of Robotics Research*, vol. 32, no. 1, 2013.

[36] Z. Artstein, "Stabilization with relaxed controls," *Nonlinear Analysis*, vol. 15, no. 11, pp. 1163–1170, 1983.